INSTITUT FÜR THEORETISCHE PHYSIK
GOETHE-UNIVERSITÄT FRANKFURT AM MAIN

BACHELOR THESIS

Phase diagram of the Gross-Neveu model from lattice calculations

Laurin Pannullo

Frankfurt am Main

Updated version from March 6, 2019 with minor corrections.

Advisor and first supervisor
Prof. Dr. Marc Wagner
Institut für Theoretische Physik
Goethe-Universität Frankfurt am Main

Second supervisor
Prof. Dr. Andreas Wipf
Theoretisch-Physikalisches-Institut
Friedrich-Schiller-Universität Jena

Selbstständigkeitserklärung

Hiermit erkläre ich, dass ich die Arbeit selbstständig und ohne Benutzung anderer als der angegebenen Quellen und Hilfsmittel verfasst habe. Alle Stellen der Arbeit, die wörtlich oder sinngemäß aus Veröffentlichungen oder aus anderen fremden Texten entnommen wurden, sind von mir als solche kenntlich gemacht worden. Ferner erkläre ich, dass die Arbeit nicht - auch nicht auszugsweise - für eine andere Prüfung verwendet wurde.

Frankfurt, den 6. September 2018 _____

(Laurin Pannullo)

Abstract

In this work the phase diagram of the 1+1 dimensional Gross-Neveu model will be investigated at finite number of quark flavors for which lattice simulations will be employed. The behavior of this system will be compared to the large-N_f results and the final result is the homogeneous phase diagram of this theory.

Zusammenfassung

In dieser Arbeit wird das Phasendiagramm des 1+1 dimensionalen Gross-Neveu Modells bei endlicher Quarkflavoranzahl untersucht. Dies wird mit Hilfe von Gittersimulationen erreicht. Das Verhalten dieses System wird mit den Ergebnis von large-N_f Rechnungen verglichen und das finale Ergebnis ist das homogene Phasendiagramm.

Contents

Chapter 1

Introduction

The 1+1 dimensional Gross-Neveu model is probably the most simple toy model for QCD one can formulate. Its Lagrangian features - besides a free Dirac part - a quartic fermion interaction term. This term approximates the fermions interactions, which are mediated by a gauge field in QCD, by a direct point interaction. That the theory is asymptotically - like QCD - was found in a large-N_f expansion [1]. A discrete chiral symmetry is realized within the model, which breaks spontaneously. A first attempt to solve the phase diagram of this symmetry breaking with a homogeneous mean field approximation yielded a homogeneous broken and restored phase [2]. The broken phase is located in the region of low temperature and chemical potential. This was, however, revised almost 20 years later using a numerical implementation of the Dirac-Hartree-Fock method and later by analytical means. An additional third crystal phase where the chiral condensate had a spatial dependence with a kink-antikink shape was found. [3]. Lattice calculations produced a similar phase diagram although with finite size artifact in the homogeneous phase [4]. All of these findings were done in the large-N_f limit.

It is now an interesting task to study this homogeneous phase diagram as a preparation and then if the inhomogeneous phase remains at finite N_f. In order to do so we will perform lattice field simulations. It is not clear if the inhomogeneous phase remains when they are subject to thermal and quantum fluctuations. Unfortunately the investigation of the inhomogeneous phase will not be achieved within this thesis. If we were to find this phase, it would be worth investigating more sophisticated models. These could be the NJL (has a γ_5 interaction term) or the Thirring model (features a continuous chiral symmetry) and they would give us further hints about the situation in QCD. Since no first principle approaches for QCD, that can explore the phase diagram in the expected region of the inhomogeneous phase, are known at this time, these hints are very valuable.

Chapter 2

Gross-Neveu model

First, we want to have a look at the 1+1 dimensional Gross-Neveu model. The Lagrangian for the Minkowski action consists of a common Dirac part and a four fermion interaction term:

$$\begin{aligned}\mathscr{L} &= \bar{\psi}_f(i\partial\!\!\!/ - m)\psi_f + \frac{g^2}{2}(\bar{\psi}_f\psi_f)^2 \\ &= \bar{\psi}_f(i\partial\!\!\!/ - m)\psi_f + \frac{\lambda}{2N_\mathrm{f}}(\bar{\psi}_f\psi_f)^2\end{aligned} \tag{2.1}$$

with $\lambda = N_\mathrm{f} g^2$ being the rescaled coupling. In the limit of $m \to 0$ (which we will assume from now on and drop the mass term) it is invariant under a discrete chiral transformations.

$$\psi \to \gamma_5\psi, \quad \bar{\psi} \to -\bar{\psi}\gamma_5 \tag{2.2}$$

Therefore the model is suited for the investigation of the spontaneous breaking of chiral symmetry, where the chiral condensate $\langle\bar{\psi}\psi\rangle$ can exhibit a nonzero vacuum expectation value. [5]

We now apply a wick rotation to the action by transforming the time coordinate as $t \to -i\tau$.

$$\begin{aligned}iS &= i\int \mathrm{d}X\left(\bar{\psi}_f(i\partial\!\!\!/)\psi_f + \frac{\lambda}{2N_\mathrm{f}}(\bar{\psi}_f\psi_f)^2\right) \\ &\xrightarrow{\text{Wick}} i\int(-i\mathrm{d}\tau)\,\mathrm{d}x\left(\bar{\psi}_f((i^2\partial_0\gamma_0 - i\partial_1\gamma_1))\psi_f + \frac{\lambda}{2N_\mathrm{f}}(\bar{\psi}_f\psi_f)^2\right) \\ &= -\int \mathrm{d}^2x\left(\bar{\psi}_f((\partial_0\gamma_{E,0} + \partial_1\gamma_{E,1}))\psi_f - \frac{\lambda}{2N_\mathrm{f}}(\bar{\psi}_f\psi_f)^2\right) \\ &= -S_\mathrm{E}\end{aligned} \tag{2.3}$$

with $\gamma_{\mathrm{E},0} = \gamma_0$ and $\gamma_{\mathrm{E},1} = i\gamma_1$.

Therefore the eulidean Lagrange density is

$$\begin{aligned}\mathscr{L}_{\mathrm{E}} &= \bar{\psi}_f((\partial_0\gamma_{\mathrm{E},0}+\partial_1\gamma_{E,1})+m)\psi_f - \frac{\lambda}{2N_{\mathrm{f}}}(\bar{\psi}_f\psi_f)^2 \\ &= \bar{\psi}_f(\partial\!\!\!/_{\mathrm{E}}+m)\psi_f - \frac{\lambda}{2N_{\mathrm{f}}}(\bar{\psi}_f\psi_f)^2 \end{aligned} \tag{2.4}$$

From here on we will drop the subscript E and assume all objects are euclidean until denoted otherwise.

2.1 Bosonization via a Hubbard-Stratonovich transformation

The four fermion interaction poses a problem for numerical lattice calculations since the fermion fields are Grassmann valued. With the help of a so called Hubbard-Stratonovich (HS) transformation we can reduce the four fermion part to a term quadratic in the fermion fields and an additionally bosonic part. The transformation is basically a shifted gaussian integral. We will use the following integral identity:

$$\exp\left(\frac{1}{2}\vec{J}A^{-1}\vec{J}\right) = \sqrt{\frac{\det A}{(2\pi)^N}}\int \mathrm{d}^N\vec{r}\,\exp\left(-\frac{1}{2}\vec{r}A\vec{r}+\vec{J}\cdot\vec{r}\right) \tag{2.5}$$

Now we want to transform the four fermion part of our action with this identity.

$$\begin{aligned}&\exp\left[\int \mathrm{d}^2x\,\frac{\lambda}{2N_{\mathrm{f}}}\left(\bar{\psi}^f\psi^f\right)^2\right] \\ &= \lim_{\substack{N_t,N_x\to\infty\\ \tau,a\to 0}} \exp\left[\sum_{i=0}^{N_t}\sum_{j=0}^{N_x}\frac{\lambda}{2N_{\mathrm{f}}}\left(\bar{\psi}^f_{i,j}\psi^f_{i,j}\right)^2\right] \\ &= \lim_{\substack{N_t,N_x\to\infty\\ \tau,a\to 0}} \left\{\sqrt{\frac{N_{\mathrm{f}}}{2\pi\lambda}}^{(N_t\cdot N_x)}\int\left(\prod_{i=0}^{N_t}\prod_{j=0}^{N_x}\mathrm{d}\sigma_{i,j}\right)\exp\left[\sum_{i=0}^{N_t}\sum_{j=0}^{N_x}\left(-\frac{N_{\mathrm{f}}}{2\lambda}\sigma^2_{i,j}-\bar{\psi}^f_{i,j}\sigma_{i,j}\psi^f_{i,j}\right)\right]\right\} \\ &= \mathscr{N}\int \mathrm{D}\sigma\exp\left[-\int \mathrm{d}^2x\left(\frac{N_{\mathrm{f}}}{2\lambda}\sigma^2+\bar{\psi}_f\sigma\psi_f\right)\right]\end{aligned} \tag{2.6}$$

with a and τ being the spacing of our intermediately discretized space and time. $\psi_{i,j}$ denotes the field at the i-th position in time and the j-th position in space. From line two to three we used eq. 2.5.

The path integral assumes the form

$$Z = \mathscr{N}\int \mathrm{D}\psi_f\,\mathrm{D}\bar{\psi}_f\mathrm{D}\sigma\exp\left[-\int \mathrm{d}^2x\left(\bar{\psi}_f\mathrm{D}\psi_f+\frac{N_{\mathrm{f}}}{2\lambda}\sigma^2\right)\right] \tag{2.7}$$

with $D = \partial\!\!\!/ + m + \sigma$. Here σ is a scalar boson field whose expectation value is linked to that of the chiral condensate. To get this relation we start with the expectation value of the chiral condensate

$$
\begin{aligned}
&\langle\bar{\psi}(X)\psi(X)\rangle \\
&= \frac{1}{Z_\psi}\int \mathrm{D}\psi_f\,\mathrm{D}\bar{\psi}_f\;\bar{\psi}(X)\psi(X)\;\exp\left[-\int \mathrm{d}^2x\left(\bar{\psi}_f\partial\!\!\!/\psi_f - \frac{\lambda}{2N_\mathrm{f}}(\bar{\psi}_f\psi_f)^2\right)\right] \\
&= \frac{1}{Z_\psi}\lim_{\substack{N_t,N_x\to\infty\\ \tau,a\to 0}}\int\left(\prod_{i=0}^{N_t}\prod_{j=0}^{N_x}\mathrm{d}\bar{\psi}^f_{i,j}\mathrm{d}\psi^f_{i,j}\right)\bar{\psi}^f_{k,l}\psi^f_{k,l}\exp\left[-\sum_{i=0}^{N_t}\sum_{j=0}^{N_x}\left(\bar{\psi}^f_{i,j}\partial\!\!\!/\psi^f_{i,j} - \frac{\lambda}{2N_\mathrm{f}}(\bar{\psi}^f_{i,j}\psi^f_{i,j})^2\right)\right] \\
&= \frac{1}{Z_\sigma}\lim_{\substack{N_t,N_x\to\infty\\ \tau,a\to 0}}\int\left(\prod_{i=0}^{N_t}\prod_{j=0}^{N_x}\mathrm{d}\bar{\psi}^f_{i,j}\,\mathrm{d}\psi^f_{i,j}\,\mathrm{d}\sigma_{i,j}\right)\left(\frac{N_\mathrm{f}}{2\pi\lambda}\right)^{(N_t\cdot N_x)/2}\frac{-N_\mathrm{f}}{\lambda}\sigma_{k,l} \\
&\quad \exp\left[-\sum_{i=0}^{N_t}\sum_{j=0}^{N_x}\left(\bar{\psi}^f_{i,j}(\partial\!\!\!/ + \sigma_{i,j})\psi^f_{i,j} + \frac{N_\mathrm{f}}{2\lambda}\sigma^2_{i,j}\right)\right] \\
&= \frac{1}{Z_\sigma}\mathcal{N}\int \mathrm{D}\psi_f\,\mathrm{D}\bar{\psi}_f\mathrm{D}\sigma\,\frac{-N_\mathrm{f}}{\lambda}\sigma(X)\,\exp\left[-\int \mathrm{d}^2x\left(\bar{\psi}_f(\partial\!\!\!/ + \sigma)\psi_f + \frac{N_\mathrm{f}}{2\lambda}\sigma^2\right)\right] \\
&= \frac{-N_\mathrm{f}}{\lambda}\langle\sigma(X)\rangle
\end{aligned}
\tag{2.8}
$$

The indices k and l correspond to the spacetime position X. Z_ψ is the normal path integral before the HS transformation and Z_σ being the transformed path integral according to eq. 2.6. From line two to three eq. 2.5 was used again for all but a single factor. For the k,l factor the following identity was used

$$
x\exp\left(ax^2\right) = \frac{1}{\sqrt{4\pi a}}\frac{-1}{2a}\int_{-\infty}^{\infty}\mathrm{d}y\,y\exp\left(-\frac{1}{4a}y^2 - xy\right) \tag{2.9}
$$

Eq. 2.8 shows the direct correspondence of the expectation value of the chiral condensate and that of sigma.

2.2 Symmetry breaking

The so called effective action S_eff is obtained when integrating out the fermion fields in eq. 2.7 and raising the resulting determinant back in the exponent.

$$
S_\mathrm{eff} = N_\mathrm{f}\left(\int \mathrm{d}^2x\frac{1}{2\lambda}\sigma^2 - \ln(\det(D))\right) \tag{2.10}
$$

This action has a single minimum in the restored phase at $\sigma = 0$. If we increase the coupling λ for a given cutoff up to a critical λ_crit, the minimum will split into two minima symmetric around the origin for homogeneous σ resulting in a non-zero vacuum expectation value of the sigma field and hence of the chiral condensate.

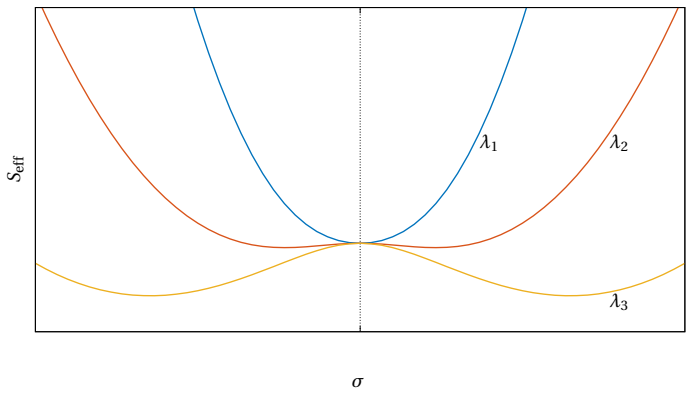

Figure 2.1: S_{eff} for homogeneous σ for different lambda. $\lambda_1 < \lambda_{\text{crit}} \lessapprox \lambda_2 \ll \lambda_3$

2.3 Phase diagram in the large-N_f limit

The GN phase diagram in the large-N_f limit consists of three phases: a homogeneous broken, restored and inhomogeneous phase. The homogeneous phases are separated by a second order phase transition up to a tricritical point. After this point the inhomogeneous phase occurs which is seperated from the other phases by phase boundaries of first order. A third phase occurs in the large-N_f limit called the inhomgenous phase. In this phase σ is a function of the position in space. For fixed T and increased μ the frequency becomes larger and the amplitude smaller as seen in fig. 2.2b. This way the phase transitions to the restored phase.

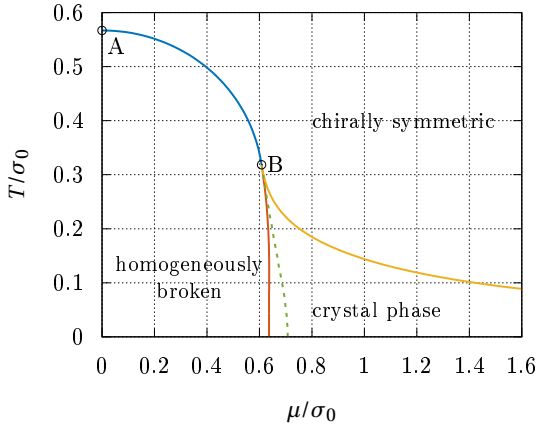

(a) Revised phase diagram of the Gross-Neveu model. A: Critical temperature, B: tricritical point, blue line: second order homogeneous phase boundary, orange/yellow line: phase boundaries of the inhomgeneous phase, dashed green line: the former phase first order boundary from Wolff. [3]

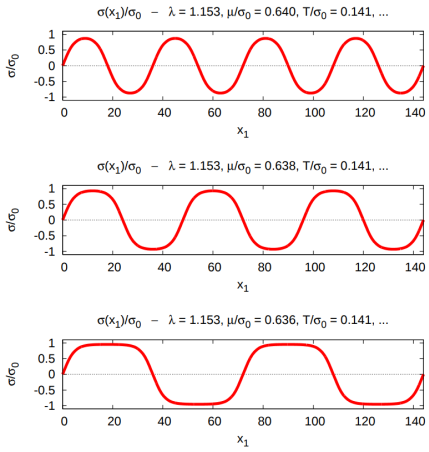

(b) The shape of the chiral condensate for $T/\sigma_0 = 0.141$ and different values of μ/σ_0. [6]

Chapter 3

Lattice field theory techniques

3.1 Pseudofermions

After the HS transformation the path integral has the following form

$$Z = \mathcal{N} \int \mathrm{D}\sigma \, \mathrm{D}\psi_f \, \mathrm{D}\bar{\psi}_f \exp\left[- \int \mathrm{d}^2 x \left(\frac{N_\mathrm{f}}{2\lambda} \sigma^2 + \bar{\psi}_f D \psi_f \right) \right] \tag{3.1}$$

which contains a quadratic fermion term. If we carry out the ψ and $\bar{\psi}$ integral we obtain the following

$$Z = \mathcal{N} \int \mathrm{D}\sigma \, \det(D)^{N_\mathrm{f}} \exp\left[- \int \mathrm{d}^2 x \, \frac{N_\mathrm{f}}{2\lambda} \sigma^2 \right] \tag{3.2}$$

This determinant is possibly difficult and/or expensive to evaluate. To circumvent this we apply a method called pseudofermions. The idea is that we raise the determinant back up in the exponent by a reverse integration of a bosonic field.

Since $\det(D)$ is real - which is shown in Appendix A - we can write

$$\det(D)^{N_\mathrm{f}} = \det(D^\dagger D)^{N_\mathrm{f}/2} = \det(M)^{N_\mathrm{f}/2} = \frac{1}{\det(M^{-r})^{N_\mathrm{PF}}} \tag{3.3}$$

with a new matrix $M = D^\dagger D$. By defining M this way we ensure that it is positive definite which is needed for the gaussian integral to converge. The number of pseudofermions is arbitrary but will be set to $N_\mathrm{f} = N_\mathrm{PF}$ and therefore $r = 1/2$ [7].

If we now perform this reverse gaussian integration over a bosonic field, we end up with the following expression for the path integral

$$Z = \mathcal{N} \int \mathrm{D}\sigma \, \mathrm{D}\phi^\dagger \, \mathrm{D}\phi \, e^{-S[\sigma, \phi, \phi^\dagger]} \tag{3.4}$$

with

$$S = S_\sigma + S_{\mathrm{PF}} = \int \mathrm{d}^2x \, \frac{N_\mathrm{f}}{2\lambda}\sigma^2 + \int \mathrm{d}^2x \, \phi^\dagger M^{-r} \phi \tag{3.5}$$

3.2 Naive discretization

The naive discretization is arguably the most simple way to discretize a derivative. We simply transform the derivative to a finite difference of the adjacent latticepoints.

$$\partial_\mu \psi(x) \to \frac{\psi_{n+\hat{e}_\mu} - \psi_{n-\hat{e}_\mu}}{2a} \tag{3.6}$$

where n is a superindex that denotes the position in spacetime. Hence $n+\hat{e}_\mu$ is the lattice point adjacent to the point n in the μ direction. ψ_n corresponds to $\psi(x)$ and a is the lattice spacing.

This discretization is hermitian, local and obviously still preserves chiral symmetry. Fermion doublers are occurring with a factor of 2 per dimension.

The operator D from eq. 2.7 takes on the following form with the naive discretization

$$D_{n,m} = \gamma_0 \frac{\delta_{n+\hat{e}_0,m} - \delta_{n-\hat{e}_0,m}}{2a} + \gamma_1 \frac{\delta_{n+\hat{e}_1,m} - \delta_{n-\hat{e}_1,m}}{2a} + \delta_{n,m}\sigma_n \tag{3.7}$$

In this discretization the chemical potential is introduced with an exponential function in the time derivative in the following way [12]

$$D_{n,m} = \gamma_0 \frac{\delta_{n+\hat{e}_0,m} \exp(\mu) - \delta_{n-\hat{e}_0,m} \exp(-\mu)}{2a} + \gamma_1 \frac{\delta_{n+\hat{e}_1,m} - \delta_{n-\hat{e}_1,m}}{2a} + \delta_{n,m}\sigma_n \tag{3.8}$$

3.3 HMC

For the lattice simulations we want to use the Hybrid Monte Carlo algorithm. Its large advantage is that the whole lattice is updated at once, whereas in the Metropolis algorithm a large number of acceptance steps are needed for which our action and hence M^{-r} has to be evaluated. The basic principle is the reformulation of a quantum field theory path integral to a partition function known from classical mechanics in which time dimension is a space dimension as well. The fields are then evolved via Hamiltonian equations of motion in a so called Molecular dynamics time. This creates a new configuration of the whole lattice. In the following discussion all fields and operators are already discretized on the lattice.

First, we introduce canonically conjugate momenta for the σ-field and can thus formulate a

Hamilton function:

$$H\left[\sigma,\pi,\phi,\phi^\dagger\right] = \sum_i \frac{1}{2}\pi_i^2 + S\left[\sigma,\phi,\phi^\dagger\right] \tag{3.9}$$

where i is a superindex that runs over all lattice sites and π being the canonically conjugate momenta for σ. We could introduce canonically conjugated momenta for the pseudofermion fields as well and evolve them, but there exists a faster way of generating configurations for them. We would now integrate over this momentum field in the continuous path integral as well:

$$Z = \mathcal{N}' \int \mathrm{D}\sigma\, \mathrm{D}\pi\, \mathrm{D}\phi^\dagger\, \mathrm{D}\phi\, e^{-H[\sigma,\pi,\phi,\phi^\dagger]} \tag{3.10}$$

These introduced momenta only change the normalization constant of the path integral, since they do not appear in any physical observable and separate as a simple Gaussian integral.

The Hamiltonian equations of motion for the fields are then:

$$\dot{\sigma}_i = \frac{\partial H}{\partial p_i}, \quad \dot{\pi}_i = \frac{\partial H}{\partial \sigma_i} \tag{3.11}$$

In order to integrate these equations of motion a set of initial field configurations is needed. The initial configuration of σ can be chosen rather arbitrarily and will only affect the time the system needs to thermalize. The initial momenta fields π are picked from a gaussian distribution. For the pseudofermions we take a look at their distribution which is proportional to

$$\exp\left[-\phi^\dagger M^{-r}\phi\right] = \exp\left[-\xi^\dagger\xi\right] \tag{3.12}$$

with $\xi = M^{-r/2}\phi$. Thus we can obtain ϕ with $\phi = M^{r/2}\xi$. Where ξ is simply a gaussian distrbuted field, which we can generate easily[8].

We can integrate the equations of motion with a symplectic integrator (e.g. leapfrog). These integrators preserve phase space area and are reversible in time, which is needed for the detailed balance of the markov chain [9]. They conserve energy up to $\mathcal{O}(\delta\tau^2)$ - with $\delta\tau$ being the integrations step size. It is also possible to integrate on multiple timescales. This means that we can integrate certain parts of our force on larger timesteps, if they do not contribute much to the overall force of the molecular dynamic. In our application this is the case for the S_{PF} part of our action S. Using this technique we can reduce the times we need to evaluate M^{-r}.

An integration of these equations of motion for a certain time will produce a new configuration. To eliminate any systematic errors we introduce a Metropolis acceptance step with the

acceptance probability:

$$P_{\mathrm{A}}\left((\sigma,\pi)\to(\sigma',\pi')\right)=\min\left(1,e^{-H[\sigma,\pi,\phi,\phi^\dagger]}/e^{-H[\sigma',\pi',\phi,\phi^\dagger]}\right) \tag{3.13}$$

with the primed fields being the evolved fields. After this we generate new momenta and pseudofermion fields and iterate this whole process until we obtained enough configurations.

Acceptance rates depend of course on $\delta\tau$ and will drop with an increased step size, since the error of the energy is larger. Though, there is also the possibility for the integrator to become unstable. Additionally the acceptance rate can vary as a function of the integration length. These two effects can be seen in a very simple quantum mechanical example with the action $S=\frac{1}{2}q^2$ in fig. 3.1. In this particular example the integrator becomes unstable for $\delta\tau=2$, because then the eigenvalues of the linear mapping of the integrator become real and increase the error exponentially.

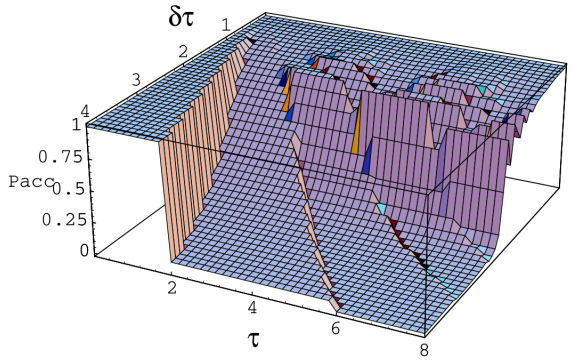

Figure 3.1: Acceptance rate for a single mode as a function of the MD step size $\delta\tau$ and trajectory length τ (rounded to the nearest integer multiple of $\delta\tau$) [10].

3.3.1 rHMC

The rational Hybrid Monte Carlo modifies the original HMC algorithm in such a way that the rational powers of M, which are needed for the algorithm, are computed with the approximation:

$$M^{-r}\approx\alpha_0+\sum_{r=1}^{N_{\mathrm{R}}}\alpha_r(M+\beta_r)^{-1} \tag{3.14}$$

where α_0, α_r and β_r are coefficients, which have to be calculated beforehand with the Remez algorithm for example. The accuracy of the approximation 3.14 is governed by the accuracy up to which the coefficients are calculated and the number of summands N_{R}. The inversions needed are done with a so-called CG multishift solver. This is a CG method, that performs the inversion for all β_r shifts at the same time [11].

Chapter 4

Observables

Our goal is to observe the different phases in the phase diagram. For this we need observables to differentiate the phases from one another and also to detect where a phase transition is happening.

4.1 Homogeneous phases

4.1.1 Order parameter

The chiral condensate $\langle\bar{\psi}\psi\rangle$ is suited to differentiate between the homogeneous broken phase and the restored phase. It can be calculated by taking the trace over the inverse Dirac operator [12]

$$\langle\bar{\psi}\psi\rangle = \frac{1}{V} tr\left[D^{-1}\right] \tag{4.1}$$

This is however quite expensive to calculate, but fortunately there exists the correspondence between $\langle\sigma\rangle$ and $\langle\bar{\psi}\psi\rangle$ that we have shown in eq. 2.8. This observable is easier to obtain since it is the field that we simulate and therefore we just have to calculate the mean of our configurations. However, $\langle\sigma\rangle$ is not suited as an order parameter observable because of the situation depicted in fig. 2.1 and the way the HMC algorithm works. The configurations will not only fluctuate around one minimum but will also be able to tunnel to the other minimum which is of the same magnitude but with opposite sign. This is especially the case for $\lambda \gtrapprox \lambda_{\text{crit}}$ since there the potential barrier is relatively small. This can be seen in fig 4.1. An average taken over all these configurations will result in $\langle\sigma\rangle \approx 0$.

A suitable alternative is $\langle|\sigma|\rangle$ as it will not experience the same annihilation as $\langle\sigma\rangle$, since - graphically spoken - all the negative values in fig 4.1 are flipped to the positive side before

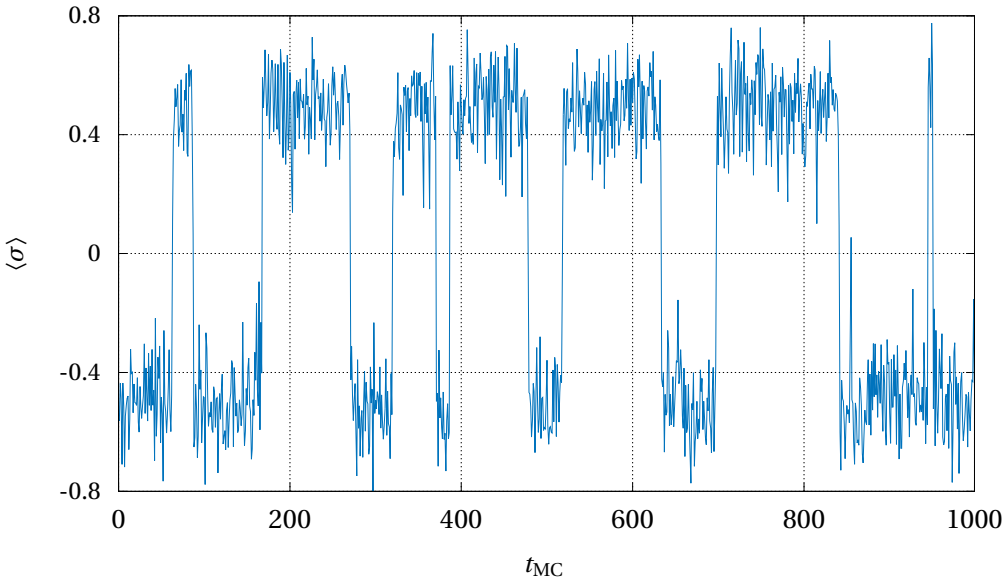

Figure 4.1: $\langle\sigma\rangle$ for every configuration of an HMC simulation with $\lambda \gtrapprox \lambda_{crit}$

taking the average. The drawback is, of course, that - even in the restored phase - $\langle|\sigma|\rangle$ will always be larger than zero. This is due to all the quantum fluctuations around the single minimum which do not annihilate each other anymore when taking the average.

4.1.2 Susceptibility

To detect a phase transition we rely on the susceptibility χ_σ of $|\sigma|$ which diverges (peaks in the finite volume case) at a phase transition. It is defined as

$$\chi_\sigma = \langle\sigma^2\rangle - \langle|\sigma|\rangle^2 \tag{4.2}$$

4.2 Inhomogeneous phase

Of course, a different observable is needed to detect the inhomogeneous phase, since its space dependency would get lost completely in $\langle|\sigma|\rangle$. An option would be the mean of a single lattice point $\langle\sigma(x)\rangle$. But it might be possible that there occurs a phase shift between configurations and hence $\langle\sigma(x)\rangle \approx 0$. An observable that preserves the oscillating properties is the following

$$P(x) = \int \mathrm{d}y \, \langle\sigma(y)\sigma(x+y)\rangle \tag{4.3}$$

To test this observable a thousand configurations of artificial data, that mimics the expected inhomogeneous phases, were generated. This data was a sinus overlayed with a noise and a

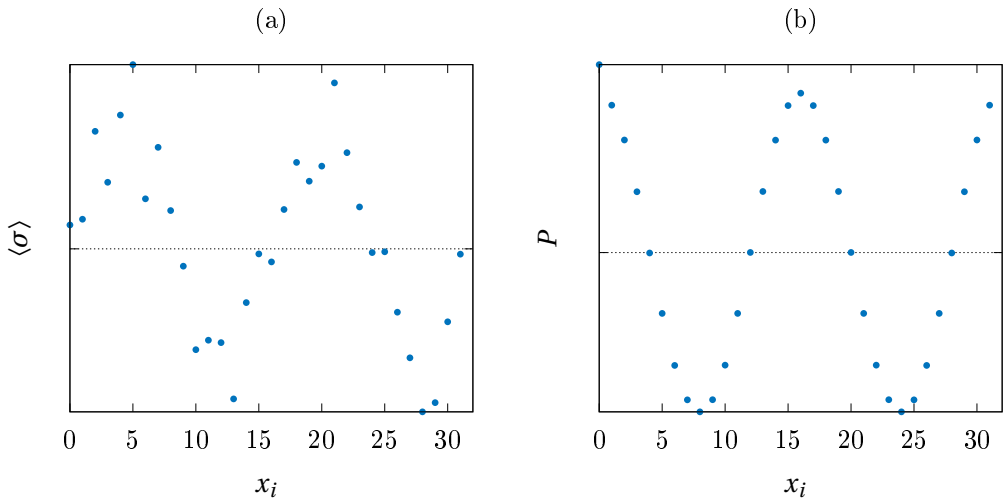

Figure 4.2: (a): A single configuration of the generated data , (b): The observable P of the generated data.

running phase shift from one configuration to another on lattice with a spatial size of 32.

The observable preserves the nature of the data although it might distorts the shape of the condensate. In contrast it is zero or constant nonzero for data that mimics the restored or broken phase. Since these tests are promising we will use this observable in the search for the inhomogeneous phase.

Chapter 5

Results

At first we are going to analyze some preliminary results, which show how the system behaves in general. Following that, the homogeneous phase diagram will be presented.

All of the following lattice simulations were done using a simulation code provided by Bjoern Wellegehausen, which has been modified by Daniel Schmidt to simulate four fermion interacting theories. All error estimates are done with the Jackknife method. The results for the large-N_f case were obtained with a code provided by Marc Wagner. Calculations on the FUCHS-CSC high-performance computer of the Goethe University Frankfurt were conducted for this research.

5.1 Coupling scans on a small lattice

In the first simulation we fix the spatial size L_s and temporal size L_t to 8 and the chemical potential μ is set to 0. Then we do a parameter scan over λ for different N_f and include the large-N_f result for comparison. The results are presented in fig 5.1.

Now there are several things to observe. Firstly, with increasing N_f and for large λ the simulation results seem to approach the infinite-N_f result with a similar linear behavior for all N_f. A large difference occurs for small λ where $\langle|\sigma|\rangle \neq 0$ for the simulations, because all the fluctuations around one minimum will not cancel each other. Also the rise of $\langle|\sigma|\rangle$ happens later than for the large-N_f result.

We can see a peak in the susceptibility. We interpret the corresponding λ as λ_crit for which the phase transition is happening at this temperature and $\mu = 0$. The system is very unstable at this coupling, which results in a larger error. For increasing N_f the height of the susceptibility's peak decreases and the critical coupling becomes smaller converging towards the critical coupling of the large-N_f result.

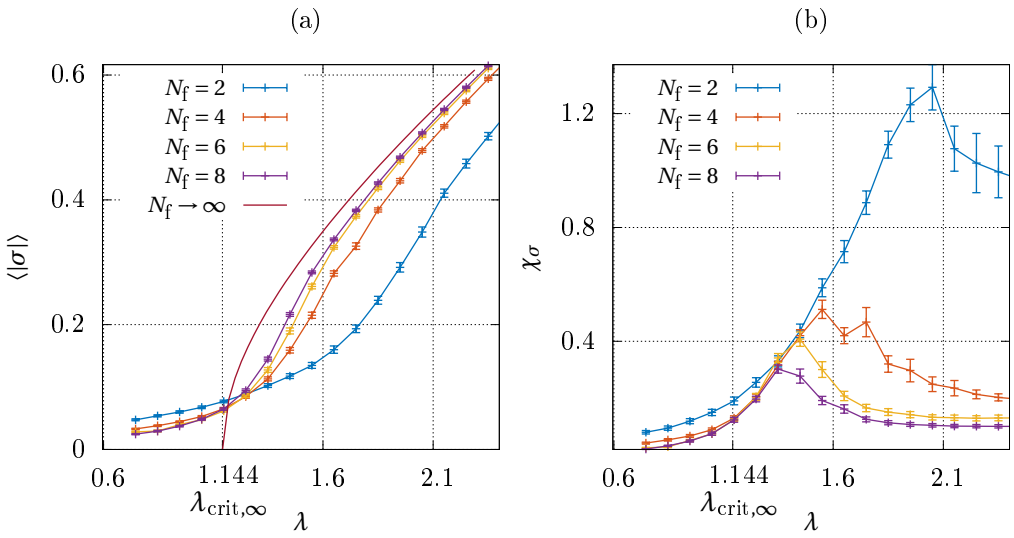

Figure 5.1: λ-scan of $\langle|\sigma|\rangle$ and χ_σ on an 8x8 Lattice for various N_f.

5.2 Dependence of the critical coupling on the spatial size

Next we want to look how the critical coupling scales with the spatial size of the Lattice. This helps us to choose the spatial size for the simulations of the entire phase diagram in a way to have a good approximation of the infinite volume limit. Scans over the coupling near λ_{crit} were performed for different spatial size at $N_f = 4$ and $L_t = 4$. Its results are presented in fig. 5.2. The peak of the susceptibility becomes larger for increasing L_s. This is expected since the susceptibility should diverge in an infinite volume. The critical coupling seems to be the same for $L_s = 32$ and $L_s = 24$. The simulation for $L_s = 32$ had some problems for smaller λ. We can neglect these, as they are far off from the peak and do not interfere with the result. For the homogeneous phase diagram we will choose $L_s = 32$, so that we do not run into problems for larger L_t.

5.3 Homogeneous phase diagram

Now we want so simulate the entire homogeneous phase diagram. As already mentioned we will do this on a lattice of $L_s = 32$ and $N_f = 4$. In preparation we need to do a λ-scan with $L_t = 4$ to determine λ_{crit}. This L_t will correspond to our critical temperature at $\mu = 0$ through the relation $T = 1/L_t$. Now we are able to scan the phase diagram in the T, μ- plane. For this we fix the coupling to the λ_{crit} obtained from the previous simulation. To scan over the temperature we vary L_t. In addition we scan over μ, which we can put in directly. The simulations with different L_t need individual adjustment of the simulation parameters since acceptance rates would fall and auto correlation would increase, if we keep the same values as for a L_t of 4.

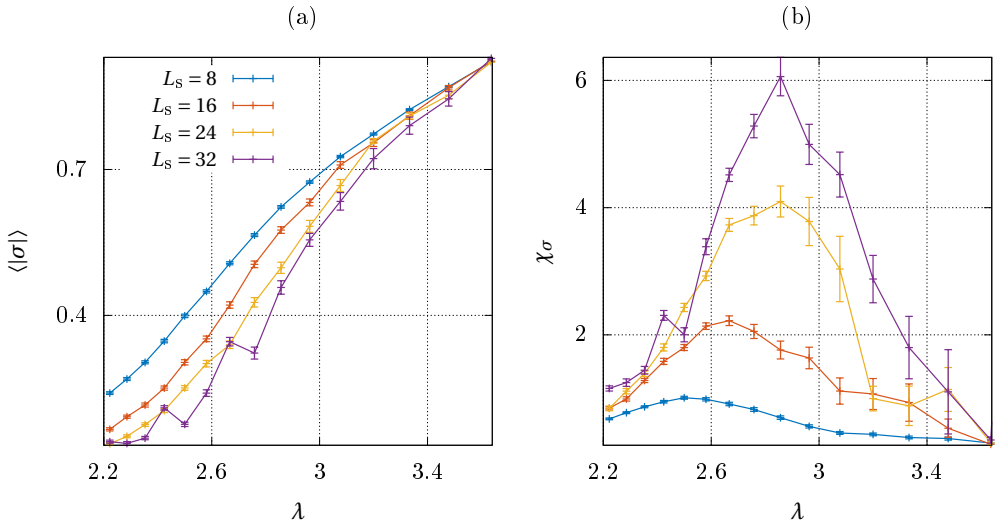

Figure 5.2: λ-scan of $\langle|\sigma|\rangle$ and χ_σ on Lattices with different spatial sizes N_s and fixed temporal size $N_t = 8$.

The T and μ axis are rescaled by σ_0. This is the $\langle|\sigma|\rangle$ value at very low temperatures and $\mu = 0$. In fig. 5.3 the value of $\langle|\sigma|\rangle$ is plotted as a heatmap. The T and μ position of a data point is indicated by the white dot and the surrounding rectangle has the corresponding color of the value of that data point. The rectangle stretches half-way to next value in all directions. The size of the squares reduces for decreasing temperature, because of the way the temporal size and the temperature are related. In fig. 5.4 the susceptibility is plotted which provide an indication on the phase boundary.

Three datapoints in the lower left corner of the plots are corrupted. The simulations were affected by autocorrelation effects which resulted in a lower value of $\langle|\sigma|\rangle$ than the expected one. It was not possible to find suitable simulation parameters in a reasonable timeframe. Therefore we will ignore these points in the discussion.

We now want to do a comparison of this simulation result for $N_f = 4$ and the analytical large-N_f result as seen in fig. 2.2a. The analytical phase boundary of the homogeneous phase is represented by the orange line. At first the region of the broken phase does not seem to match in T direction. This occurs, because the value of σ_0 in the simulations differs from the infinite-N_f result. It would match, if we would rescale by the σ_0 of the infinite-N_f result. In the μ-direction the phase boundaries seem to match quite well.

From the two phase boundaries of the suspected inhomogeneous phase only the one to the broken phase is visible. It is not as sharp as the phase boundary between the broken and restored phase, but runs in a similar manner as in the large-N_f result. To sum it up it can be said that the phase diagram takes on a similar form as in the large-N_f case.

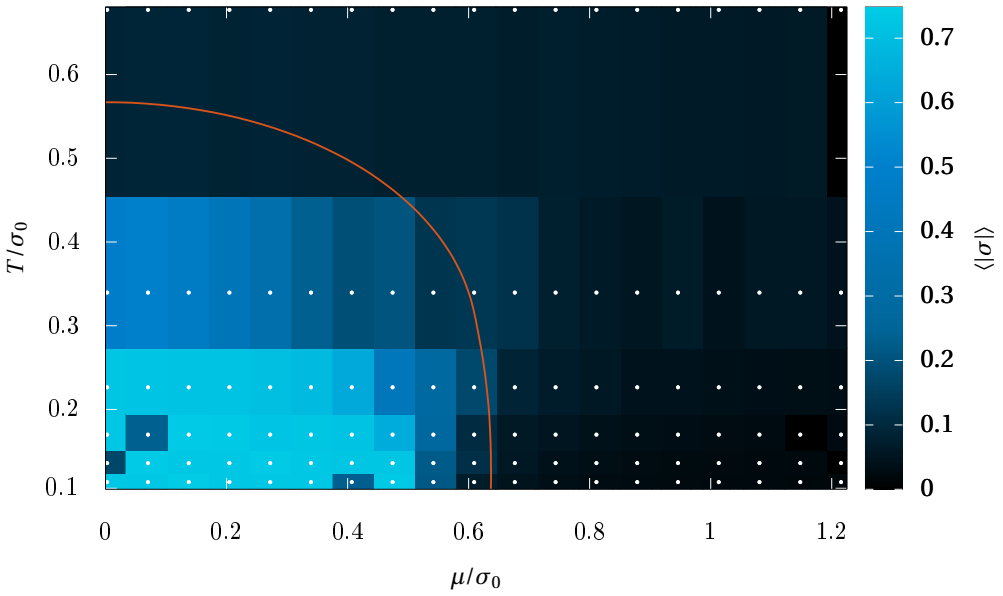

Figure 5.3: $\langle|\sigma|\rangle$ in the T, μ- plane on a $L_s = 32$ lattice and for $N_f = 4$.

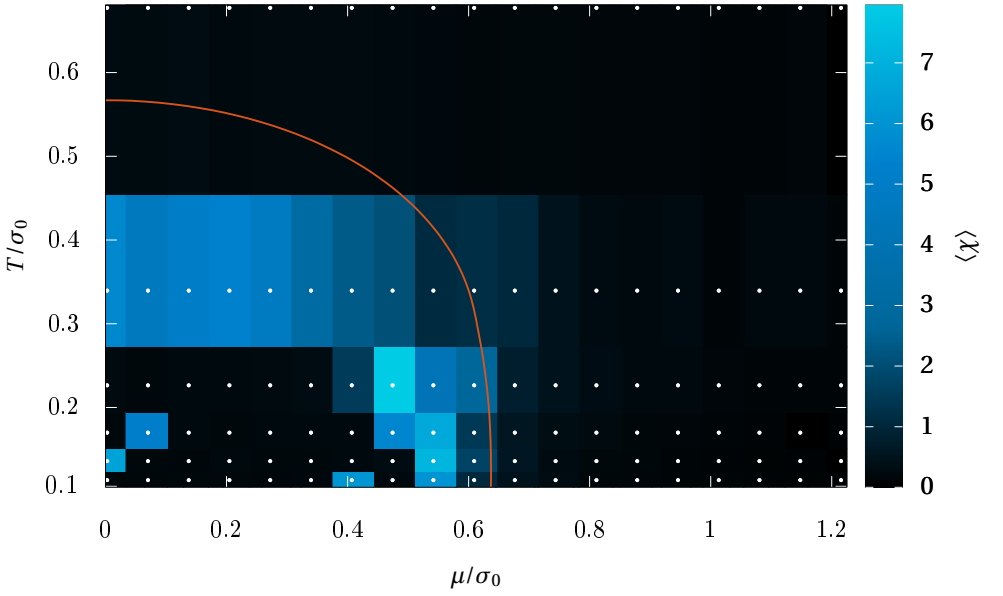

Figure 5.4: χ_σ in the T, μ- plane on a $L_s = 32$ lattice and for $N_f = 4$.

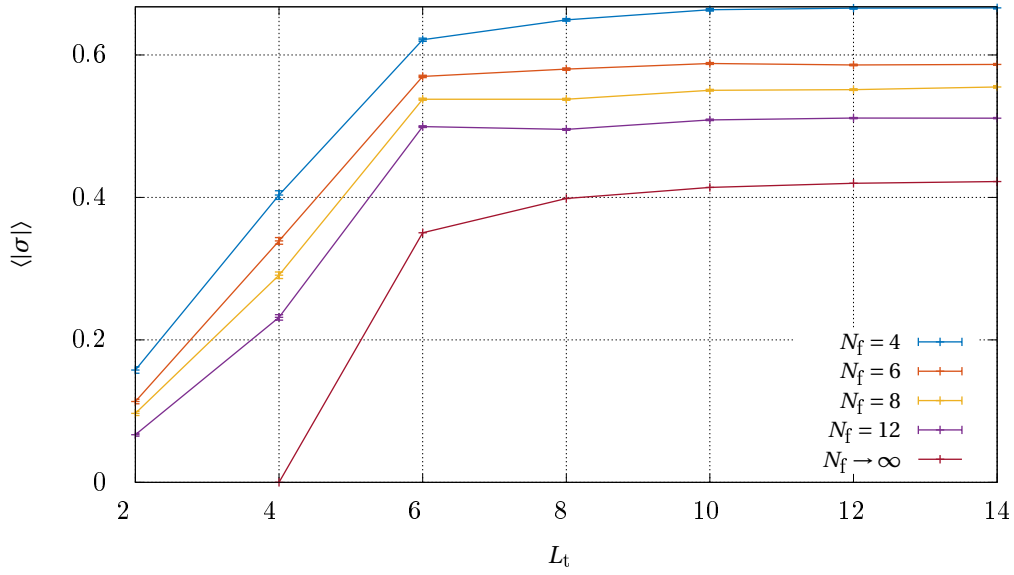

Figure 5.5: Scan of $\langle|\sigma|\rangle$ over L_t for different N_f.

5.4 Temperature scans at vanishing chemical potential

As we have observed earlier, the phase diagram for $N_f = 4$ is distorted in the temperature direction, because - amongst other things - the value of σ_0 is larger than that in the large-N_f case. It would be interesting to observe the dependence of σ_0 on N_f. To achieve this, simulations at $\mu = 0$ and for different N_f and L_t on a $L_s = 8$ were performed. The coupling was tuned so that the phase transition happens at $L_t = 4$. By increasing L_t we lower the temperature. This small lattice was chosen, because it was difficult to tune the parameters for larger N_f on bigger lattices and calculations would have taken a lot longer. This does not pose a problem, since we only want to observe a trend.

For large L_t we are deep in the homogeneous broken phase and $\langle|\sigma|\rangle$ approaches σ_0. As we can observe, the value of σ_0 scales indeed with N_f and converges to the value of the large-N_f result. This encourages that the homogenoues phase diagram will converge to that of the large-N_f result for increasing N_f.

Chapter 6

Conclusion

6.1 Summary

The simulations, that were done, served primarily to get acquainted with the lattice techniques and program at hand. However there were also some physical relevant findings. The most important one is that the theory shows behavior similar to a phase transition even for finite N_f. The fact that the behavior of the system converges for increasing N_f to that of the large-N_f case is relieving. Thus we know that there is no drastic change of physics in the large-N_f results and the more physical situation of finite N_f is still relevant. Therefore an occurrence of the inhomogeneous phase at finite N_f is still plausible.

6.2 Outlook

Based on these findings the next task will be to simulate the phase diagram at larger N_f to get closer to the large-N_f result. The difficulty to overcome here is to determine the correct simulation parameters for which the simulation still runs in a reasonable time. Following that, one can implement the previously discussed observable for the inhomogeneous phase. If this phase is found, it is reasonable to simulate other models which resemble QCD more closely. If they are not found, it might be worth investigating this phase in 2+1 or 3+1 dimensions. It is possible that one might encounter a sign problem in 2+1 dimensions. This is subject to further investigations, if needed.

Appendix A

Proof that det(D) is real in 1+1 dimensions

In even dimensions the irreducible gamma matrices are unique up to a similarity transformation. γ_μ^* also fulfills the Clifford algebra and hence is related to γ_μ through a similarity transformation [13]:

$$\gamma_\mu^* = B\gamma_\mu B^{-1} \tag{A.1}$$

We now take a look at the eigenvalue equation of D

$$\left(\gamma_0\partial_0 + \gamma_1\partial_1 + \sigma\right)\psi = \lambda\psi \tag{A.2}$$

If we take the complex conjugate of this and apply A.1 we obtain

$$\left(B\gamma_0 B^{-1}\partial_0 + B\gamma_1 B^{-1}\partial_1 + \sigma BB^{-1}\right)\psi^* = \lambda^*\psi^* \tag{A.3}$$

and after a multiplication with B^{-1}:

$$\left(\gamma_0\partial_0 + \gamma_1\partial_1 + \sigma\right)B^{-1}\psi^* = \lambda^* B^{-1}\psi^* \tag{A.4}$$

Now we have another eigenvalue equation of D. Since D is two dimensional in spinor space, it will have two eigenvalues for every spacetime position. The determinant is the product of all eigenvalues. So either λ is complex and therefore $\det(D)$ is the absolute squared of λ or λ is real and $\det(D)$ is again real.

Bibliography

[1] D. J. Gross and A. Neveu, Phys. Rev. D **10**, 3235 (1974).

[2] U. Wolff, Phys. Lett. B **157**, 303 (1985).

[3] M. Thies and K. Urlichs, Phys. Rev. D **67**, 125015 (2003) [hep-th/0302092].

[4] P. de Forcrand and U. Wenger, PoS LATTICE **2006**, 152 (2006) [hep-lat/0610117].

[5] V. Schön and M. Thies, In *Shifman, M. (ed.): At the frontier of particle physics, vol. 3* 1945-2032 [hep-th/0008175].

[6] M. Wagner, Phys. Rev. D **76**, 076002 (2007) [arXiv:0704.3023 [hep-lat]].

[7] D. Schmidt, Phd thesis (2018)

[8] H. J. Rothe, World Sci. Lect. Notes Phys. **74**, 1 (2005)

[9] A. D. Kennedy, [hep-lat/0607038].

[10] R. G. Edwards, I. Horvath and A. D. Kennedy, Nucl. Phys. B **484**, 375 (1997) [hep-lat/9606004].

[11] B. Wellegehausen, Phd thesis (2012)

[12] C. Gattringer and C. B. Lang, Lect. Notes Phys. **788**, 1 (2010).

[13] J. Park, Lecture note clifford algebra